Characteristics of Rainfall and Convection and Synoptic Conditions of Mesoscale Convective Systems at Yangtze-Huai River Basin: Contrasting Meiyu with Pre- and Post-Meiyu Periods

Hui Wang, Yali Luo*, Renhe Zhang

State Key Laboratory of Severe Weather, Chinese Academy of Meteorological Sciences, Beijing, China

*** Email: yali_luo@hotmail.com**

1. Objective

To compare rainfall characteristics and convective intensity of precipitation systems over the Yangtze-Huai River Basin (YHRB; 28º-34ºN, 110º-122ºE) among the pre-Meiyu, Meiyu and post-Meiyu periods, using surface station gauge observations and TRMM datasets during 1998-2008. Efforts are also made to relate the structure and convective characteristics of mesoscale convective systems (MCSs) to synoptic conditions during the three periods.

Methodology

Start and ending dates of the Meiyu period are determined objectively for each individual year, accurately representing interannual variations of Meiyu. A RPF is defined as a contiguous area consisting of near surface raining pixels detected by TRMM PR. Based on their area and the existence of convective pixels, the RPFs are categorized into three types: MCS, sub-MCS, and non-convective system (Other).

2. Rainfall accumulation during 1998-2008

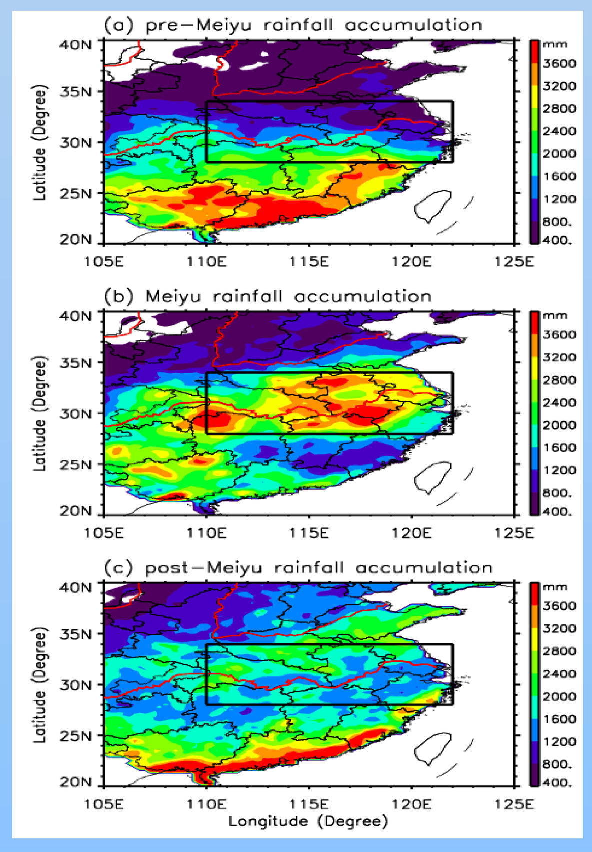

Figure 1: 11-year (1998-2008) rainfall accumulation during the periods of (a) pre-Meiyu, (b) Meiyu and (c) post-Meiyu. Red lines represent Yellow and Yangtze River, respectively. The black box represents the analysis region.

3. Population and rainfall contribution

Period	Total RPFs		MCSs (%)		subMCSs (%)		Others (%)	
	P	R	P	R	P	R	P	R
pre-Meiyu	22274	2.1	2.3	88	14.4	6	83.3	6
Meiyu	25506	4.6	3.3	91	21.6	6	75.0	3
post-Meiyu	27640	3.3	3.3	80	33.7	16	63.0	4

Table 1: Total population (P; unit: #) and near surface volumetric rain (R; unit: 10^7 mm h^{-1} km^2) of all RPFs and the relative percentages (%) from the three RPF groups (MCS, subMCS and Other) during pre-Meiyu, Meiyu and post-Meiyu periods.

4. Vertical profile of radar reflectivity

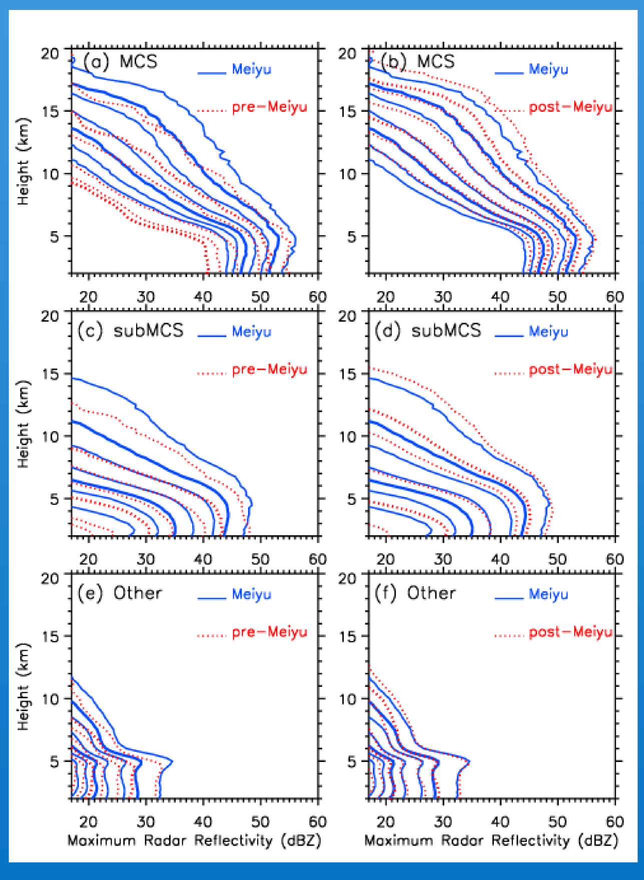

Figure 2: Vertical profiles of cumulative frequency (from left to right in 50, 60, 70, 80, 90, 95 and 99th percentile) of maximum radar reflectivity of MCS (a, b), subMCS (c, d) and Other (e, f) during the periods of Meiyu (blue lines), pre-Meiyu (dashed red lines in left panels), and post-Meiyu (dashed red lines in right panels).

5. Area and near surface volumetric rain of MCSs

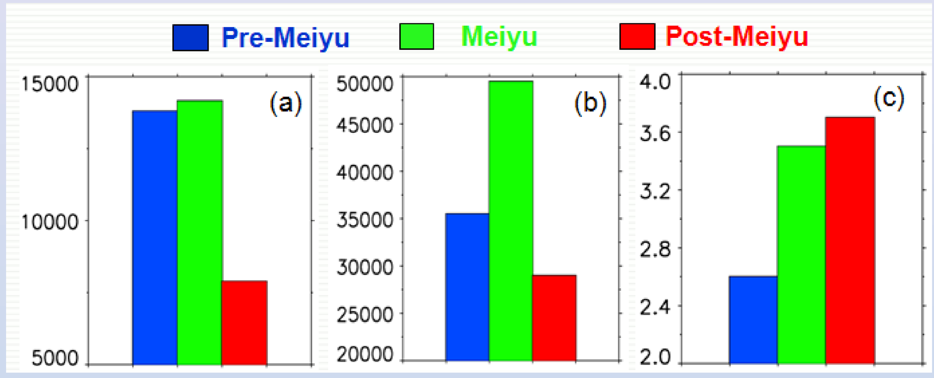

Figure 3: Mean values of area (km^2; a), near surface volumetric rain (mm h^{-1} km^2; b) and areal-averaged volumetric rain (mm h^{-1}; c) of MCSs during the periods of pre-Meiyu, Meiyu and post-Meiyu.

6. Convective intensity of MCSs

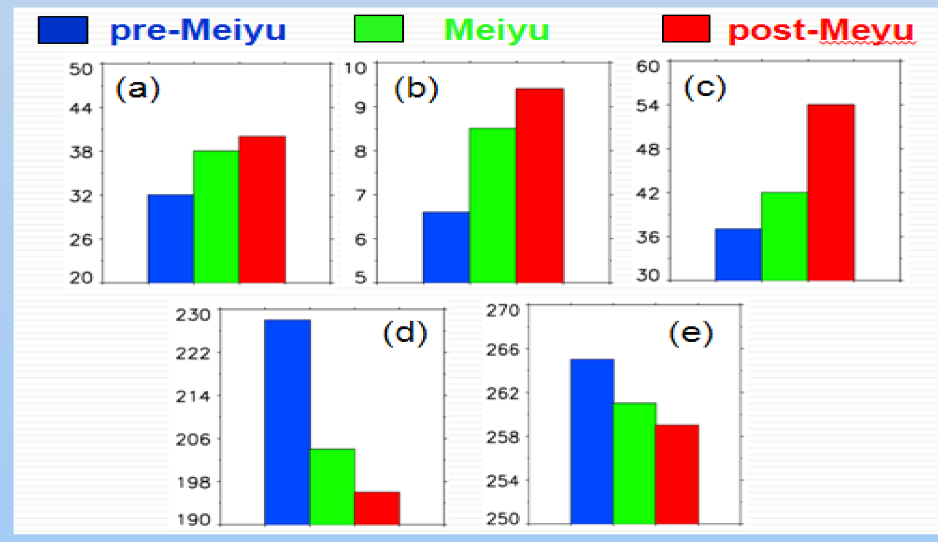

Figure 4: Mean values of maximum radar reflectivity at 6 km (dBZ; a), maximum height of 30 dBZ (km; b), lightning rate (min^{-1}; c), minimum 85 and 37 GHz PCT (K; d and e) of MCSs during the periods of pre-Meiyu, Meiyu and post-Meiyu.

7. Mean synoptic conditions of MCS

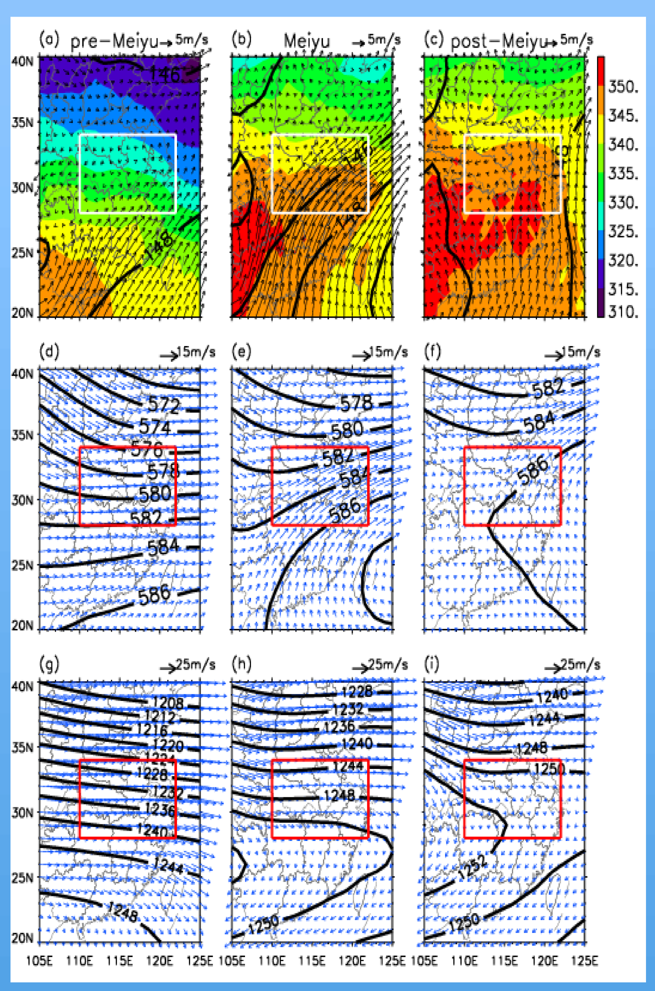

Figure 5: Horizontal wind (arrow), geopotential height (contour) and pseudo equivalent potential temperature (shading, only 850 hPa) at 850 hPa (a-c) and 500 hPa (d-f) and 200 hPa (g-i) averaged when MCS was detected by TRMM over the YHRB during the pre-Meiyu, Meiyu and post-Meiyu periods.

8. Moisture condition: MCS mean and contract between MCS and noMCS

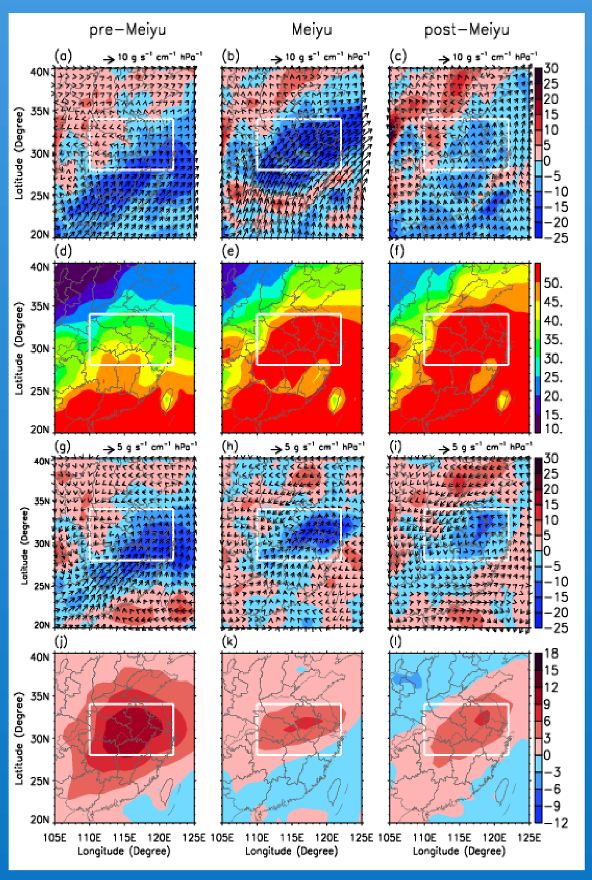

Figure 6: Convergence of water vapor flux in the entire layer (shading) and water vapor flux at 850 hPa (arrow) (a-c) and precipitable water (d-f) when MCS was detected by TRMM over YHRB during the pre-Meiyu, Meiyu and post-Meiyu periods. The corresponding MCS-noMCS contrasts are in g-i and j-l, respectively.

9. MCS-noMCS contrasts

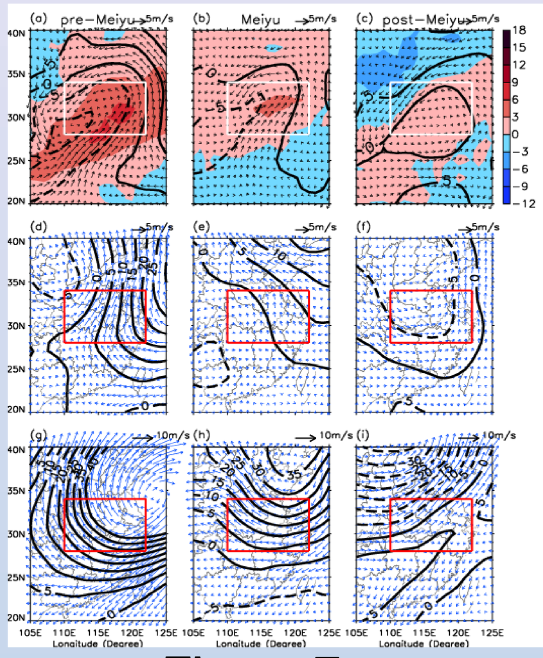

Figure 7

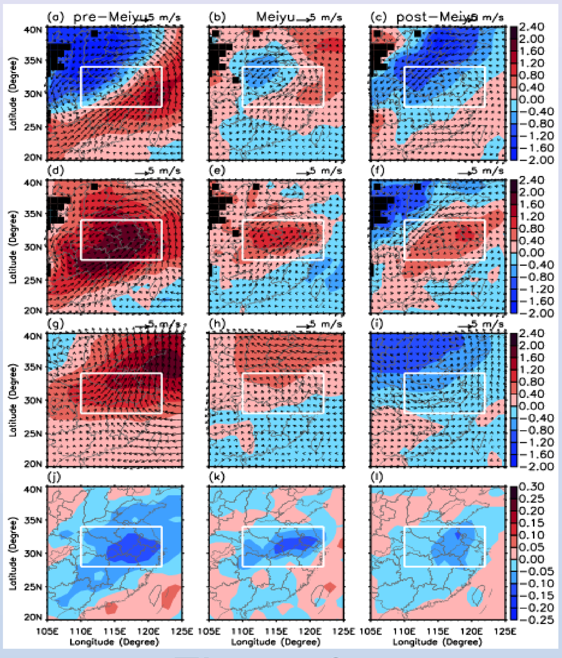

Figure 8

Figure 7: MCS-noMCS contrasts in the horizontal wind (arrow), geopotential height (contour) and pseudo equivalent potential temperature(shading, only 850 hPa) at 850 (a-c), 500 (d-f) and 200 hPa (g-i) in the pre-Meiyu, Meiyu and post-Meiyu.

Figure 8: MCS-noMCS contrasts in temperature and horizontal wind (contoured and arrow) at 850 (a-c) and 500 hPa (g-i), specific humidity at 850 hPa (d-f, contoured), and vertical velocity at 500 hPa (j-l, contoured) in the pre-Meiyu, Meiyu and post-Meiyu.

10. CAPE and diurnal variations of MCSs

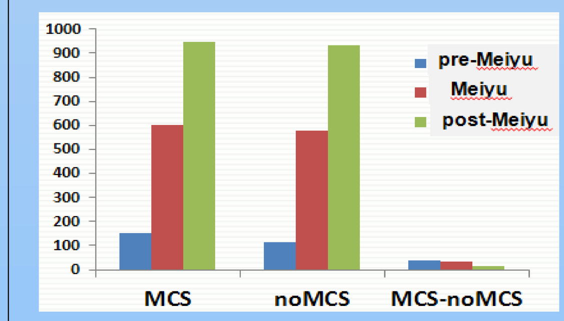

Figure 9

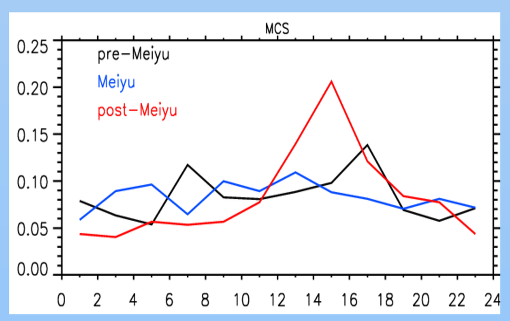

Figure 10

Figure 9: Mean values of CAPE when MCS (noMCS) was detected by TRMM over YHRB and MCS-noMCS contrasts in pre-Meiyu, Meiyu and post-Meiyu.

Figure 10: Diurnal variations of MCSs during the three periods.

11. Conclusion

- Total rainfall accumulation amount during the Meiyu period distributes quasi-west- easterly over the YHRB, with several rainfall maxima being located mostly near Mountains. In contrast, the rainfall maxima appear mainly to the south of Yangtze River during the pre-Meiyu and are located at northwestern YHRB during the post-Meiyu period.
- MCSs are the most important contributors to precipitation over the YHRB during late-spring to midsummer, contributing more than 80% to total near surface volumetric rain.
- The convective intensity of MCSs over the YHRB increases from the pre-Meiyu to Meiyu and further strengthen to the post-Meiyu period. Compared to the other two periods, weaker convection during the pre-Meiyu period is due to both less water vapor and smaller CAPE. During the post-Meiyu period intrusion of strong cold air at mid-level increases CAPE and induces the strongest convection.
- By average, horizontal sizes of MCSs during pre-Meiyu and Meiyu are comparable, being nearly twice of the post-Meiyu MCSs. That is partially because MCSs during pre-Meiyu and Meiyu are closely related to large-scale weather systems such as fronts, but are more connected with smaller-scale thermal convective systems in the afternoon during the post-Meiyu period.